A fully coupled model for predicting geomechanical and multiphase flow behaviour in fractured rocks.

HAWEZ, H.K., ASIM, T. and FAZIO, M.

2024

Unconventional Resources 4 (2024) 100105

Contents lists available at ScienceDirect

Unconventional Resources

journal homepage: www.keaipublishing.com/en/journals/unconventional-resources/

A fully coupled model for predicting geomechanical and multiphase flow behaviour in fractured rocks

Haval Kukha Hawez [a], Taimoor Asim [b,*], Marco Fazio [c]

[a] Department of Petroleum Engineering, Faculty of Engineering, Koya University, Koya, KOY45, Kurdistan Region, Iraq
[b] School of Engineering, Robert Gordon University, AB10 7GJ, UK
[c] Department of Applied Geology, University of Göttingen, Goldschmidtstraße 3, 37077, Göttingen, Germany

ARTICLE INFO

Keywords:
Fractured rocks
Fracture-matrix interface
Capillary pressure
Relative permeability
Pore pressure

ABSTRACT

Geomechanical and multiphase flow characteristics are essential in recovering oil from naturally fractured rocks during hydrocarbon production because of changes in pore pressure and tension within the rock. It is a well-established fact that the geomechanical and multiphase flow characteristics of fractured rocks are interdependent on each other. Evaluation of these characteristics, for hydrocarbons displaced by water in fractured rocks under external stress loading, is severely lacking in published literature. This study aims to develop a novel numerical framework for a fully coupled model of fractured rocks, taking into consideration the pore pressure and porous media discontinuity at the fracture-matrix interface, along with an expanded Darcy's equation. The fully coupled Finite Element Method (FEM) and Computational Fluid Dynamics (CFD) model developed in this study is shown to accurately predict geomechanical and multiphase flow behaviour at the fracture-matrix interface. The results show that as external stress loading on the fractured rock increases, the porosity and permeability of the rock matrix decrease, capillary pressure at the fracture-matrix interface decreases, and the relative permeability curves shift to the right, indicating a water-soaked fracture-matrix interface. The findings of this study can be used to develop innovative strategies for enhanced oil recovery from fractured rocks.

1. Introduction

Multiphase flow in fractured tight rocks presents a complex challenge for petroleum reservoir engineers due to the difficulty in understanding the flow behaviour at the fracture-matrix interface. Fractured tight rocks are characterised by low-permeability matrix rock with interconnected fractures that act as fluid conduits. The interaction between the matrix and fracture systems controls the flow behaviour, which the presence of multiple phases such as oil, gas, and water can further complicate. Although fractures in the tight rocks have decreased relative volumes, they nonetheless function as highly conductive flow media. The fractures of the tight rocks will dominate and regulate the single or two-phase flow because of their high permeability.

In practice, pressure and stress are dispersed non-uniformly in a tight rock, and fractures in the tight rocks cause compaction and decompaction [1]. Fracture apertures in the fractured tight rocks during single and multiphase flow have an impact on the pressure and fluid dispersion due to their high conductivity [2,3]. The coupled geomechanics and transient multiphase characterisations are a significant occurrence. It will yield a more substantial understanding of the spatiotemporal fluctuations of fluid flow behaviour in a porous media and effective stress continuously [4,5]. The flow exchange predictions are highly predominant at the fracture-matrix interface in recovering fluid from the fractured tight rocks [6,7]. The fracture-matrix interface is crucial in determining the flow behaviour in fractured tight rocks. This interface is often characterised by a complex network of more minor fractures and pores that affect the reservoir's fluid flow and transport properties [8,9]. The flow behaviour at the fracture-matrix interface is affected by a wide range of factors, such as fracture spacing, fracture aperture, matrix permeability, and the wettability of the rock surface. Multiphase flows in matrix rocks will complicate modelling fluid flow patterns and effective stress in a fractured tight rock [10,11]. In many practical situations, such as improved oil recovery and CO_2 storage, and where multiphase flow interaction occurs (i.e., between oil, water, and gas contact), multiphase flow behaviour is crucial and complicated with fractures in a fractured tight rock [12,13]. In order to optimise time and resources, alternative methodologies have been adopted in various studies, incorporating Darcy's approaches. These approaches entail modelling the mechanics of fluids and solids within porous mediums

* Corresponding author.
E-mail address: t.asim@rgu.ac.uk (T. Asim).

https://doi.org/10.1016/j.uncres.2024.100105
Received 13 December 2023; Received in revised form 26 April 2024; Accepted 26 April 2024
Available online 28 August 2024

Nomenclature

D	Diameter (cm)
L	Length (cm)
h	Fracture aperture (μm)
σ	Applied stress (MPa)
d	Displacement (μm)
S	Saturation (−)
φ	Porosity (−)
k	Permeability (mD)
Kr	Relative permeability (−)
Ψ	Source term (−)
μ	Dynamic viscosity (Pa.s)
η	Darcy velocity (m/s)
ρ	Density (kg/m^3)
ε_{vol}	Volumetric strain (−)
K_d	Drained bulk modulus (MPa)
P	Pore pressure (Pa)
e	Void ratio (−)
ν	Poisson's ratio (−)
λ_B	Biot-Willis coefficient (−)
M	Biot modulus (MPa)
Pc	Capillary pressure (kPa)

through averaged quantities, utilizing Darcy's law, pore-network models, or Biot theory [14,15]. One such strategy involves employing the Beavers-Joseph (BJ) boundary condition to link fluid flow in solid-free domains (modelled via the Navier-Stokes equations) with that in microporous domains (modelled via Darcy's law), primarily for single-phase flow and static porous media [16,17]. Recent research has expanded upon this BJ approach, enabling multiphase flow in solid-free domains [18] or incorporating poroelasticity effects within porous mediums [19]. Nonetheless, as far as our current knowledge extends, techniques capable of simultaneously coupling solid mechanics with multiphase flow across both solid-free and porous domains are severely limited in the published literature. Thus, there is a strong demand to develop reliable and well-structured numerical modelling to examine those, as mentioned earlier, complex multiphase and geomechanical processes in fractured rock.

The dual porosity/permeability model and the Discrete Fracture Model (DFM) are extensively used for characterising fractured rocks [20,21]. The first dual-continuum method evolved as the dual-porosity model for single-phase systems [22,23]. An orthorhombic continuum of fractures separates the rectilinear matrix prisms in this concept (i.e., the sugar-cube model). The reservoir is discretised into the matrix and fracture domains for dual-porosity simulation [24]. As a result, fracture and matrix pressures and saturations are present at every point in the reservoir. According to a dual-porosity model, the rock matrix is a fluid reservoir, and flow only occurs in fractures. Injection and production wells, presumptively finished in the fracture domain, have a flow route provided by interconnected fractures. The exchange term that links each fracture cell to its equivalent matrix cell in a grid block forms the connection between the matrix and fracture domains in the dual-porosity model. In order to mimic fluid flow in naturally fractured rocks, Kazemi et al. [25] and Rossen [26] expanded the Warren and Root approach to multiphase flow and created dual-porosity simulators. Since then, numerous simulators for field-scale naturally fractured rock simulations have incorporated the dual-porosity technique.

When these suppositions are considered, the dual-porosity model is a crude depiction of a geologically complicated reservoir. As a result, much work has gone into making the dual-porosity model more accurate. The MINC (multiple interacting continua) method, the subdomain method [27,28], and the pseudo capillary pressure and relative permeability techniques [29] are a few significant advancements. Furthermore, dual-permeability models have been created using the same methodology as dual-porosity models but with matrix-to-matrix flow [30,31].

Natural fractures differ significantly in height, length, aperture, spacing, and network connectivity, according to studies on outcrop characterisation [32]. This highlights a significant discrepancy between reality and the uniformity implied by dual-porosity and permeability model assumptions. In order to decrease the number of non-physical abstractions present in dual-continuum models, discrete-fracture models (DFMs) have been created [33,34]. To explicitly portray a fracture network, most DFMs rely on unstructured grids. DFMs have various benefits over dual-porosity and permeability versions. As they can model a realistic fracture system geometry, they explicitly consider how individual fractures affect fluid flow. The fracture model is easily adaptable and updatable since they are not too bound by grid-defined fracture geometry limitations. Additionally, because it directly depends on the shape of the fracture, the specification of the exchange between matrix and fracture is simpler. However, a drawback of DFMs is that they frequently result in discrete systems of equations with complicated structures and challenges in numerical solutions. Nonetheless, improvements in numerical solution techniques and the efficacy of our new methodologies have reduced this drawback. After coupling the geomechanical process, these models demonstrated a higher ability to represent the development of fluid flow distributions in natural and hydraulic fractures of the same intensity. Similarly, the fluid mass exchange from the rock matrix to the fracture depends on the rock permeability at the fracture and matrix interface. As a result, the DFM model was employed in this study to investigate the displacement of a viscous oil by water in a porous medium with fractures.

Many scholars who worked on multiphase fluid flow in porous media with geomechanics created a fully connected multiphase flow and geomechanics solution for heterogeneous media [35,36]. The numerical results were found to agree well with the analytical results. The developed simulator's synthetic application in a tight gas reservoir with gas and water saturation was investigated [37]. It was investigated that water saturation increases with the pore space of the rock as it deforms. Shen et al. [38] presented a finite difference method for modelling a fully coupled multiphase fluid flow and geomechanical processes. The technique was successfully applied to the tight gas reservoir with hydraulic fractures. It was also investigated that variations in pore pressure and temperature characteristics are essential in well-stimulation modelling. Cui et al. [39] used fully coupled two-phase flow and poromechanics modelling in COMSOL Multiphysics® to examine the influence of the geomechanical process on coal bed methane recovery. Changes in porosity, permeability, water retention, and the relative permeability curve were specifically examined as a function of effective stress and induced shrinkage. It was concluded that disregarding geomechanical effects during fluid flows in the CBM reservoir will result in excess or under-prediction of the production rate. Therefore, in the current work, we have incorporated geomechanics into our mathematical model for displacing a viscous oil by water at the fracture-matrix interface.

The geomechanical model is solved separately in the one-way coupling system, and the reservoir properties are periodically updated. Information is solely exchanged in one direction, from a geomechanical model to a fluid flow model, as the name suggests. This idea is expanded upon by two-way coupling, and the geomechanical implementation is additionally updated using the information from the fluid flow model. Frequency and data interchange are key factors in the effectiveness of one and two-way coupling methods. The iterative coupling scheme

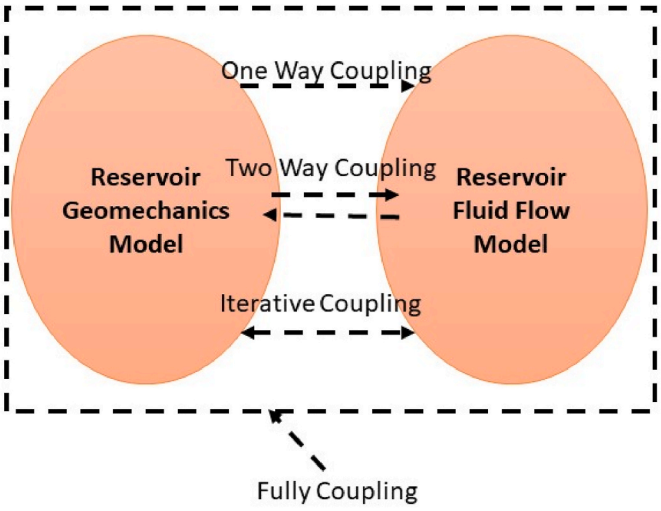

Fig. 1. Geomechanics and fluid flow coupling schemes [40].

tackles some of the challenges that various coupling techniques encounter face, such as convergence and numerical stability. These models' output might not be accurate, necessitating using concurrent (geomechanics and flow) modelling such as a fully coupled model. Fig. 1 depicts how distinct numerical coupling schemes work.

The current work focuses on developing a novel and comprehensive modelling framework that bridges the gap between geomechanics and multiphase flow at the fracture-matrix interface in fractured rocks. The fully coupled model developed in his study takes into account the pore pressure in the rock matrix and also accurately models the porous media discontinuity at the fracture-matrix interface. By considering these two critical aspects, the fully coupled model can capture the complex and dynamic interactions that govern the behaviour of fractured rocks and multiphase flow at the fracture-matrix interface.

2. Fully coupled model development

According to Darcy's law, the infused fluid is expected to flow both within the matrix and from the injection well to the production well. Equation (1) provides the overall mass conservation equation for the rock matrix's two-phase (viscous oil and water) flow [41]:

$$\frac{\partial}{\partial t}\left(\varphi\, S_\beta\, \rho_\beta\right) + \nabla.\left(\rho_\beta\, \eta_\beta\right) + \Psi_\beta = 0 \tag{1}$$

where β represents a phase, φ is the porosity, S is the saturation, ρ is the density (kg/m^3), η is the Darcy velocity (m/s) and Ψ is the source term. The Darcy velocity can be expressed as:

$$\eta_\beta = -\frac{k_a\, Kr_\beta}{\mu_\beta}\left(\nabla P_\beta - \rho_\beta\, g \nabla D\right) \tag{2}$$

where k_a is the absolute permeability (mD), Kr is the relative permeability, P is the pore pressure (Pa), g is the gravitational acceleration (m/s^2), and D is the diameter of the core region (m). Similarly, the source term (Ψ) can be written as:

$$\Psi_\beta = \rho_\beta\, \alpha_B \left(\frac{\partial \varepsilon_{vol}}{\partial t}\right) \tag{3}$$

where α_B is the Biot coefficient and ε_{vol} is the volumetric strain. In the present study, the effects of gravity are ignored and thus, the pressure gradient acts as the only driving force for the transport of oil within the core and fracture regions. The Biot modulus (M) and the Biot coefficient (α_B) can be written as:

$$\frac{\partial}{\partial t}\left(\varphi\, S_\beta\, \rho_\beta\right) = \frac{1}{M}\frac{\partial\left(S_\beta\, \rho_\beta\, p_\beta\right)}{\partial t} \tag{4}$$

$$\frac{1}{M} = \frac{\varphi}{k_f} + \left(\alpha_B - \varphi\right)\frac{1-\varphi}{K_d} \tag{5}$$

where k_f is the fracture permeability (mD) and K_d is the drained bulk modulus (MPa). Substituting equations (2)–(5) into equation (1), the governing mass conservation equation can be used for the fully coupled scheme can be expressed as:

$$\left(\frac{\varphi}{k_f} + \left(\alpha_B - \varphi\right)\frac{1-\varphi}{K_d}\right)\frac{\partial\left(S_\beta \rho_\beta p_\beta\right)}{\partial t} - \nabla.\left(-\frac{k_a Kr_\beta\, \rho_\beta}{\mu_\beta}\left(\nabla P_\beta - \rho_\beta g \nabla D\right)\right) = \rho_\beta \alpha_B \left(\frac{\partial \varepsilon_{vol}}{\partial t}\right) \tag{6}$$

where ε_{vol} is the volumetric strain.

The saturation (S), capillary pressure (Pc), and relative permeability (Kr) at the fracture-matrix interface are then calculated based on the Brooks and Corey method [42].

Based on the modified multiphase flow governing equations presented here, the poroelastic relationship between stress, strain, and pore pressure needs to be modified. This relationship can be written as:

$$\sigma = \sigma' - \alpha_B\, P_\beta\, I \tag{7}$$

where σ and σ' are total and effective stress (MPa) respectively, and I is the second-order identity tensor. The volumetric strain in equation (6) can then be expressed as:

$$\varepsilon_{vol} = \frac{1}{2}\left[\left(\nabla d\right)^2 + \nabla d\right]\ \varepsilon_{ij} = \frac{1}{2}\left(\frac{\partial d_i}{\partial x_j} + \frac{\partial d_j}{\partial x_i}\right) \tag{8}$$

where d is the displacement (cm). The force equilibrium (or solid deformation) can be represented by:

$$\nabla.\sigma + \left(\rho_\beta\, \varphi + \rho_\beta\right) g = 0 \tag{9}$$

Porosity is conventionally obtained through physical testing such as saturation tests [43]. As the core undergoes compaction, its porosity (φ) changes due to the volumetric strain (ε_{vol}), resulting in geometric variations in the pore spaces, while the solid regions remain intact. The porosity of the sample can be obtained through constitutive models, such as [44]:

$$\varphi = \frac{e}{1+e_i} = \frac{e_i - \left(1+e_i\right)\varepsilon_{vol}}{1+\left[e_i - \left(1+e_i\right)\varepsilon_{vol}\right]} \tag{10}$$

As the rock undergoes compression, the ability of multiphase flow through it changes. The permeability of the rock matrix (k_{mat}) can be expressed as [45]:

$$k_{mat} = k_{i-mat}\left\{1 \pm \frac{1}{2}\left[\frac{9(1-\nu^2)}{2}\left(\frac{\pi\, \Delta\sigma}{E}\right)^2\right]^{1/3}\right\}^2 \tag{11}$$

where k_{i-mat} is the initial rock matrix permeability (mD) and E is Young's modulus (GPa) of the rock matrix. The positive sign refers to dilatational loading, and the negative signal corresponds to the compressional loading [46].

Under stress loading, the permeability of the fracture region also changes [47]. Zhang et al. [48] provide a relationship between the fracture permeability (k_f) and stress-induced fracture aperture change, which can be expressed as:

$$k_f = k_{i-f}\left(1 + \frac{\Delta h}{h_i}\right)^3 \tag{12}$$

where k_{i-f} is the initial fracture permeability (D) and Δh is the change in

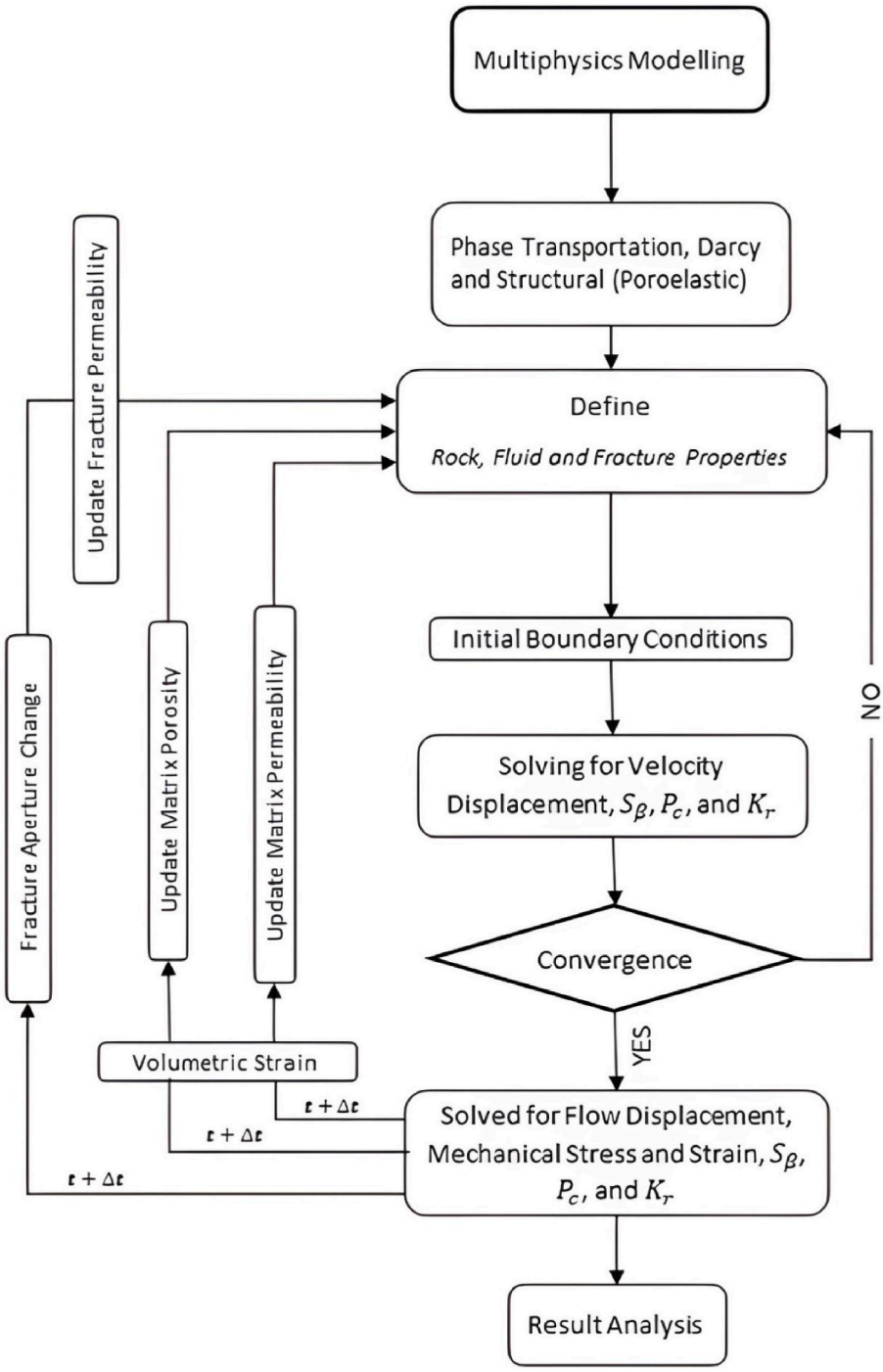

Fig. 2. The fully coupled scheme.

the fracture aperture (μm) after the application of stress i.e. $\Delta h = h_i - h$.

The Brooks and Corey method models the contact between the rock matrix and the fracture zone [42]. According to this method, the fluid saturation (S), of the phases can be expressed as:

$$S_o = \frac{(S_{io} - S_{ro})}{(1 - S_{ro} - S_{rw})} \tag{13}$$

$$S_w = \frac{(S_{iw} - S_{rw})}{(1 - S_{ro} - S_{rw})} \tag{14}$$

where the subscripts i and r represent initial and residual respectively.

The Brooks and Corey method is used to compute the capillary pressure as a function of water saturation at the fracture matrix interface, which can be expressed as:

$$Pc = Pec\ S_w^{-1/\lambda_p} \tag{15}$$

where Pec is the entry capillary pressure (Pa) and λ_p is the pore size distribution index.

The relative permeability is computed as a function of the water saturation and pore size distribution index (λ_p) using the Brooks and Corey method, as expressed below:

$$Kr_w = S_w^{(3+2/\lambda_p)} \tag{16}$$

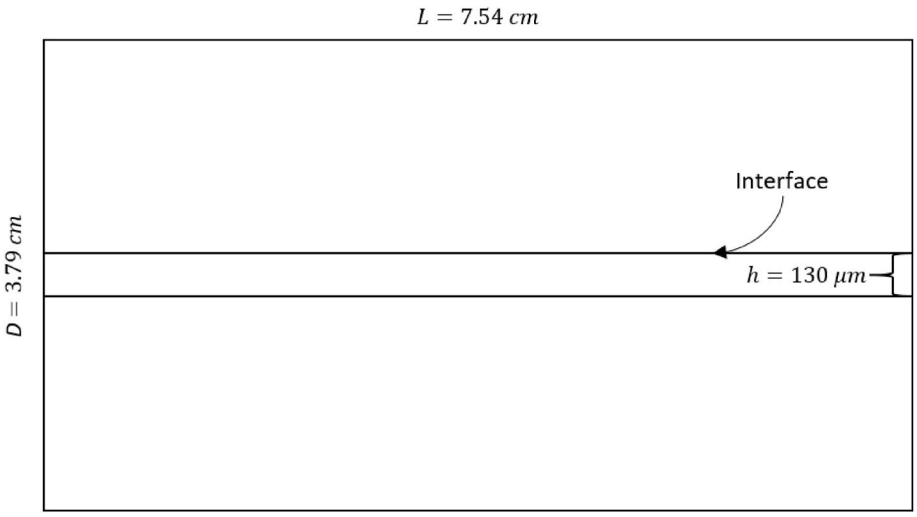

Fig. 3. 2D Geometry of fractured rock.

$$Kr_o = (1 - S_w)^2 \left(1 - S_w^{\left(1+2/\lambda_p\right)}\right) \quad (17)$$

2.1. Numerical solution strategy

This work studies coupled geomechanics and transient two-phase fluid flow in naturally fractured rocks using COMSOL Multiphysics 6.0, with both the core and fracture zones modelled as porous media. Poroelastic and multiphase modules, i.e., coupled modules for Darcy's law, solid mechanics, and phase transportation, have been used. A fracture in a porous material is modelled in the solid mechanic's module as a thin elastic layer border element with varying fracture properties. As a result, the integrated fracture boundary condition was applied to the fractures in Darcy's law module. The integrated fracture boundary condition provides a more realistic and accurate model for analysing fractures in solid materials and is an important tool in fractured rocks. The flow chart representing the implementation of the fully coupled scheme is shown in Fig. 2.

Variations in the petrophysical and geomechanical properties (i.e., equations (10)–(12)) are explicitly considered dynamic local variables. At each time step's convergence, the generated strain in the rock matrix and fracture is used to update porosity values (equation (10)); the updated porosity values are then used to compute the elastic modulus spatially (equation (10)). The volumetric strain affects the permeability of the rock matrix (equation (11)). On the other hand, the fractures' permeability is determined by the stresses (equation (12)). These updated values are input in the part that defines the property after each time step $(t + \Delta t)$.

The Backward Differentiation Formula (BDF) solver is an implicit solver that applies one to five backward differentiation formulas depending on the accuracy level. One to five backward differentiation formulas refer to numerical methods used for solving ordinary differential equations (ODEs) or partial differential equations (PDEs) [49]. Lower-order techniques can provide significant dampening. The Backward Euler method substantially muffles any high frequencies [50]. Notwithstanding the damping in Backward Euler, a solution with steep gradients may finally yield a reasonably smooth solution. Variable order is thus employed in COMSOL's BDF implementation. In other words, high demand will be employed wherever possible, and a lower order will be automatically picked to achieve stability. A low-order technique is used for attenuating oscillations or instabilities in the numerical solution of a dynamic [51]. As a result, the implicit BDF was applied for time-step discretisation. The Newton nonlinear technique was used with the MUMPS (Multifrontal Massively Parallel Direct Solver) to solve the nonlinear system of equations with a pivoting perturbation of 12 - 10. A mapped quadrilateral mesh is used because it provides better accuracy and convergence rates for many problems, especially those involving anisotropic materials or complex geometries; it allows for easy implementation of boundary conditions and has a lower computational cost than unstructured meshes, which is based on transfinite interpolation.

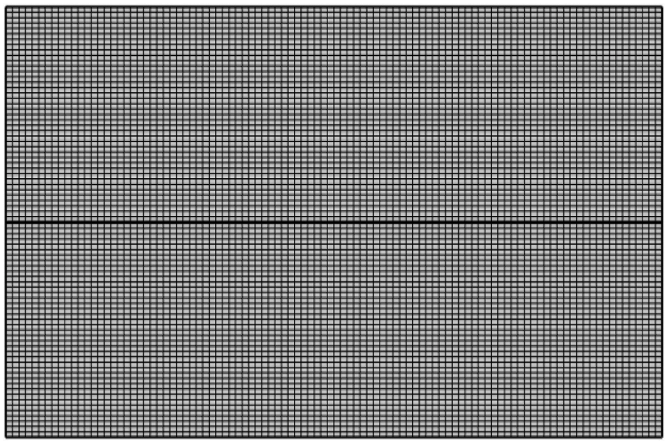

Fig. 4. Mesh within the fractured rock.

3. Numerical modelling of fractured rocks

3.1. Geometry and meshing of the tight rock

Fig. 3 displays the 2D geometry of the discrete fracture matrix model (DFM) for the naturally fractured rock. The geometric model is based on Clashach Core Flooding experiments [45,52], and thus, the core's diameter (D) and length (L) are 3.79 cm and 7.54 cm, respectively. The initial aperture size (h) of the rectangular fracture in the center of the core sample is 130 μm [40]. The 2D geometric model has been selected for analysis in this study, instead of a 3D model, because the 2D model can accurately mimic the geomechanical and multiphase flow behaviour within the fractured rocks, while significantly reducing the computational expense. Moreover, as the flow through the fractured rock is expected to be laminar, considering a 2D geometric approach is reasonable in the absence of Reynold stresses.

A structured quadrilateral mesh has been generated in the flow domain in order to reduce numerical errors and enhance prediction

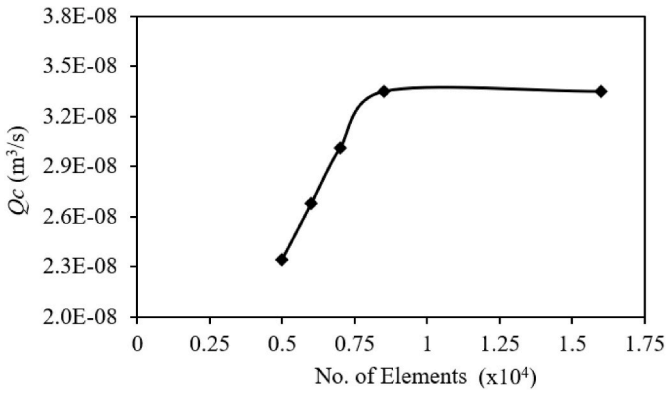

Fig. 5. Mesh independence test results.

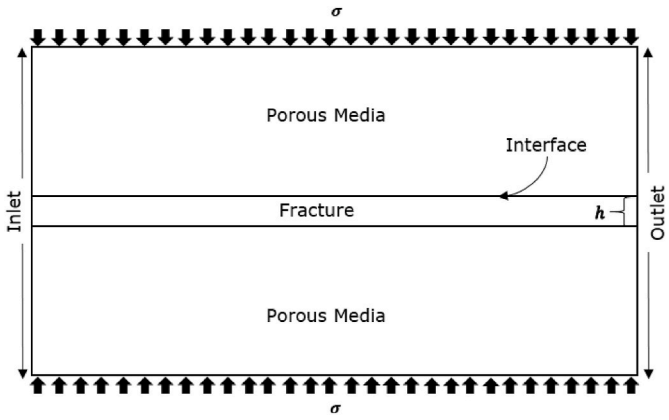

Fig. 6. 2D model of fractured rock under different stress loading.

accuracy [11]. With regards to mesh sizing, 80 elements are specified in the radial direction (excluding the aperture), while 100 elements are specified in the axial direction of the fractured rock sample. To accurately capture the complex geomechanical and multiphase flow behaviour within the fracture region, 5 mesh elements have been in the cross-section. The resulting mesh comprises 0.85×10^4 elements and is shown in Fig. 4.

In order to ascertain that the numerically predicted results presented in this study are independent of the mesh sizing used, five other meshes were also generated and tested for cumulative discharge of oil (Qc), the same parameter that has been used later on for validating the numerical model of this study against the published experimental data. The range of the total number of mesh elements in these meshes is $0.5 \times 10^4 - 1.6 \times 10^4$. The results for the mesh independence tests are shown in Fig. 5. It can be seen that as the number of elements increases from 0.5×10^4 to 0.85×10^4, the cumulative oil discharge increases, while between 0.85×10^4 and 1.6×10^4, there is negligible difference in the cumulative oil discrage. Thus, the mesh shown in Fig. 4, having a total number of 0.85×10^4 elements, has been chosen for further analyses in this study.

3.2. Material properties

This study focuses on porous medium modelling with a single fracture zone using a fully coupled scheme, taking into consideration the pore pressure within the rock matrix. Porosity, matrix permeability, fracture aperture, and fracture permeability have been considered as functions of pore pressure and the generated stresses in the porous media. The petrophysical properties, fracture aperture, and fracture permeability have been observed under different stress loadings, ranging from 6.9 MPa to 17.2 MPa, as shown in Fig. 6. This range of external stress loading has been considered to be the most realistic in real-world scenarios [45]. The corresponding petrophysical, fluid, fracture, and geomechanical parameters have been reported in Table 1.

Table 1
Reservoir rock, fluid, fracture, and geomechanical properties [45,52].

Parameters	Value
Pore Volume; PV (cm^3)	6.62
Pore Size Distribution Index; λ_p (−)	0.674
Entry Capillary Pressure; P_{ec} (Pa)	345
Matrix Permeability; k_{mat} (mD)	315
Matrix Porosity (−)	0.154
Fracture Permeability; k_f (D)	310
Oil viscosity (Pa.s)	0.001
Oil density (kg/m^3)	850
Young's Modulus (Pa)	40×10^9
Poisson's Ratio (−)	0.14
Rock density (kg/m^3)	2500

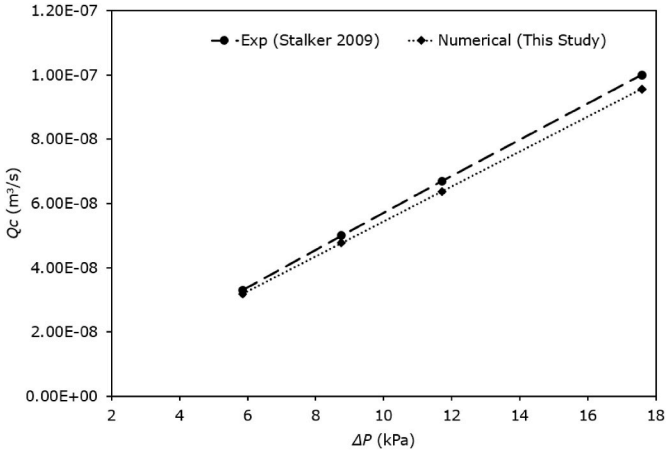

Fig. 7. Validation of the numerical model w.r.t. the experimental data.

3.3. Initial and boundary conditions

Before applying applied stress and water injection for oil recovery, it is presumed that the rock core sample contains 80 % oil and 20 % water. Particularly in fractured tight rocks, the macroscopic saturation of different phases is commonly discontinuous where the porous zones with higher and lower permeability meet. Most published studies do not consider this porous media discontinuity when simulating multiphase flow in fractured rocks [53,54]. In the present study, the Porous Media Discontinuity boundary condition has been employed, where the fracture-matrix contact is subjected to the following conditions:

$$P^l_{c\beta}\left(S^l_\beta\right) = \begin{cases} P^l_{ec,\beta} & if\ P^h_{c\beta}\left(S^h_\beta\right) \le P^l_{ec,\beta} \\ P^h_{c\beta}\left(S^h_\beta\right) & if\ P^h_{c\beta}\left(S^h_\beta\right) > P^l_{ec,\beta} \end{cases} \quad (18)$$

where the superscript h indicates the boundary's high permeability and the superscript l indicates the barrier's low permeability side. Suppose, the capillary pressure on the high permeability side is smaller than the entrance capillary pressure on the low permeability side. In this case, the saturation of the phase on the low permeability side is equal to zero (or residual saturation).

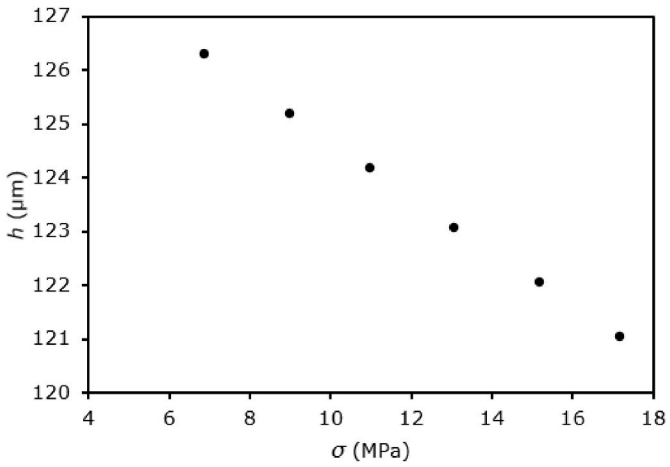

Fig. 8. Fracture aperture variations w.r.t stress loading.

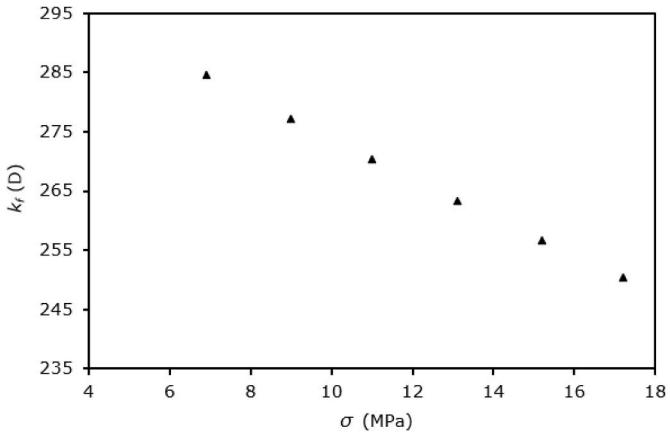

Fig. 9. Variations in fracture permeability w.r.t stress loading.

4. Results and discussions

4.1. Validation of the numerical model

The fully coupled numerical model, taking into consideration the pore pressure and porous media discontinuity, has been validated against the Clashach Core flooding experimental data [52]. The cumulative outflow results from the full coupling-based numerical model were contrasted with the single-phase flow experimental flooding data because the experimental data was unavailable. The cumulative discharge of oil (Qc) is calculated using the differential pressure (ΔP) applied across the sample reservoir. The outcomes of the numerical model validation are shown in Fig. 7. It can be seen that the differential pressure increases, so do the numerically predicted and empirically measured Qc values. The two Qc curves match well with an average difference of 4.2 %. Thus, the fully coupled model developed in the present study, considering the 2D geometric model, pore pressure, and porous media discontinuity, is capable of accurately mimicking real-world geomechanical and multiphase flow behaviour within fractured rocks.

4.2. Stress-dependent fracture properties

4.2.1. Fracture aperture

The variations in fracture aperture (h) with respect to external stress loading (σ) is shown in Fig. 8. Under no stress loading, the fracture aperture was 130 μm. It can be seen in the figure that as the rock matrix is subjected to 6.9 MPa of external stress, the fracture aperture decreases to 126.3 μm (0.87 % decrease). This decrease in the fracture aperture is due to the vertical displacement of the fracture under the action of externally applied loading, which is expected in real-world scenarios. As the stress loading increases to 9 MPa, the fracture aperture decreases to 125.2 μm, representing a further 0.87 % decrease. The same trend is observed for higher stress loading values considered in the present study, till the fracture aperture reduced to 121.1 μm, which is 6.8 % less than under no external loading. The figure shows that the fracture aperture decreases linearly with increasing stress loading until the fracture is completely closed.

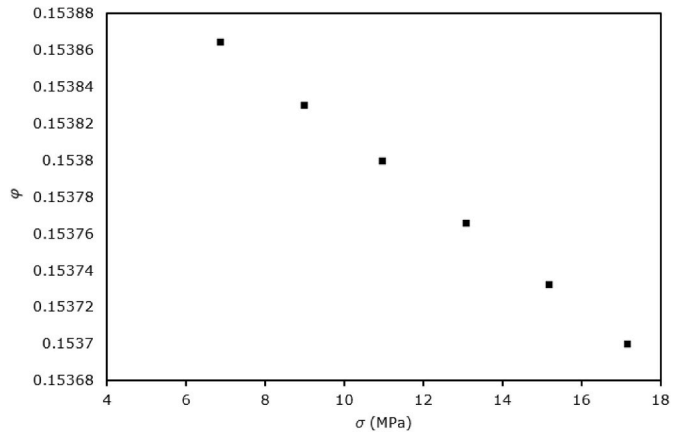

Fig. 10. Porosity variations w.r.t stress loading.

4.2.2. Fracture permeability

Stress-induced fracture permeability (k_f), based on equation (12) that provides the mathematical basis for its dependency on the fracture aperture, is depicted in Fig. 9. It can be seen that as stress loading increases, the fracture permeability decreases linearly (the same trend observed in case of fracture aperture). Under the application of a 6.9 MPa load, the fracture permeability is 285 D, which decreases to 277 D (a 2.6 % drop) when the external load increases to 9 MPa. The fracture permeability decreases by 2.4 %, 2.6 %, 2.4 %, and 2.5 %, respectively, when stress loading increases to 11 MPa, 13.1 MPa, 15.2 MPa, and 17.2 MPa respectively. As observed by Cao et al. [55], an increase in external loading contracts the fracture aperture, resulting in a lower available flow area in the fracture, thus decreasing the ability for the flow to take place. In the present study though, the accuracy of predicting the fracture permeability has been significantly enhanced by considering the pore pressure and the porous media discontinuity between the fracture and rock matrix zones, enabling the reservoir engineers to make more accurate estimations on the enhanced oil recovery from such reservoirs.

4.3. Stress-dependent petrophysical properties

4.3.1. Porosity

Application of external stress loading is expected to not only reduce the fracture aperture, and thus its permeability, but also compact the rock matrix, resulting in lower porosity (φ) and permeability (k_{mat}) in the porous zone as well [56]. In order to fully capture this effect, the matrix porosity variations under the action of externally applied stress loading have been shown in Fig. 10. It can be seen in the figure that as stress loading increases, the porosity decreases linearly. As summarised in Table 1, under no external load, the matrix porosity is 15.4 %. When subjected to a 6.9 MPa load, the rock matrix's porosity reduces to 15.386 %, which is a negligible change in the matrix porosity. Further increasing the load to 9 MPa results in a matrix porosity of 15.383 %. Under an external load of 17.2 MPa (highest load considered), the matrix porosity reduces to 15.37 %, which is 0.2 % lower than under no

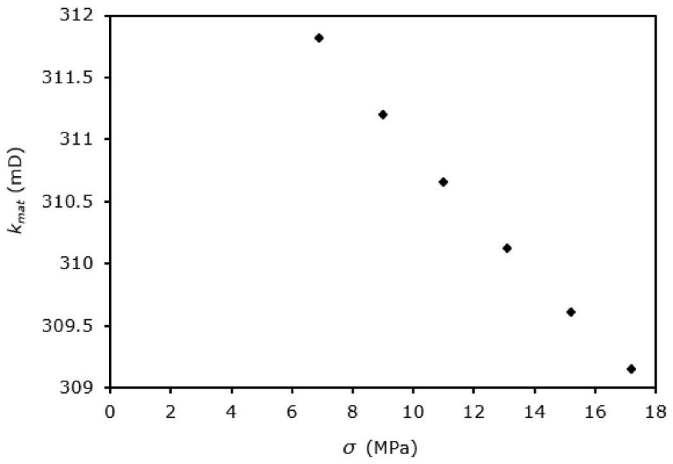

Fig. 11. Matrix permeability variations w.r.t stress loading.

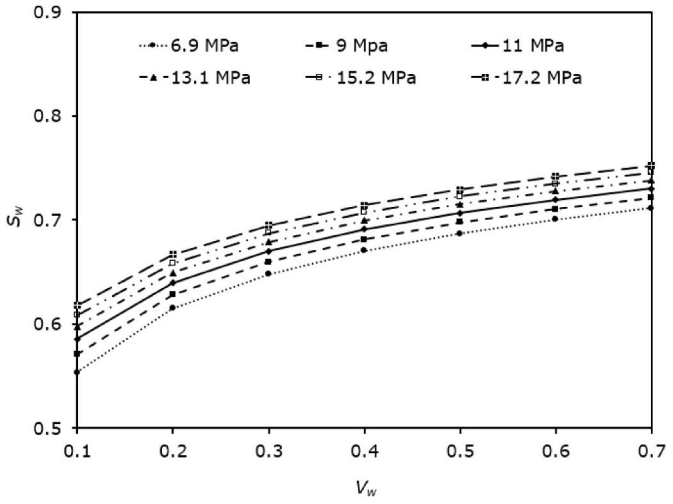

Fig. 12. Variations in water saturation at the fracture-matrix interface for different water volume injection and stress loading.

load conditions. Although for the same range of external stress loading, the fracture aperture decreases by 6.8 %, there is a very small change in the matrix porosity, and the reason for this is the stiffness of the rock matrix region, which is quite high compared to the stiffness of the fracture zone.

Although very small, a reduction in the matrix porosity leads to the deformation of the core sample, which alters the matrix pore network and pore volume. It is important to note that the impact of pore fluid compression or expansion is explicitly considered in the constitutive model developed in this study. Understanding the relationship between stress loading and matrix porosity is crucial in predicting porous materials' behaviour under stress and designing effective reservoir management strategies. The results presented in this study are crucial to advancing our understanding of the intricate relationships that exist between porosity, fluid flow, and stress in porous media, which lead to building reliable reservoir engineering techniques and further enhancing oil recovery from fractured reservoirs.

4.3.2. Matrix permeability

The variations in matrix permeability (k_{mat}) as a function of stress loading (σ) are shown in Fig. 11. As expected, a linear decrease in matrix permeability is observed when the stress loading on the rock matrix increases. Under no-load conditions, the matrix permeability is 315 mD, which decreases to 311.8 mD under a stress loading of 6.9 MPa (1 % decrease). As stress loading further increases to 9 MPa, the matrix permeability decreases to 311.2 mD (0.20 % decrease). Thus, the application of stress loading, leading to compaction of the rock matrix, results in lower matrix permeability. Under a stress loading of 17.2 MPa, the matrix permeability is 309.1 mD, which is 1.87 % lower than under no-load condition.

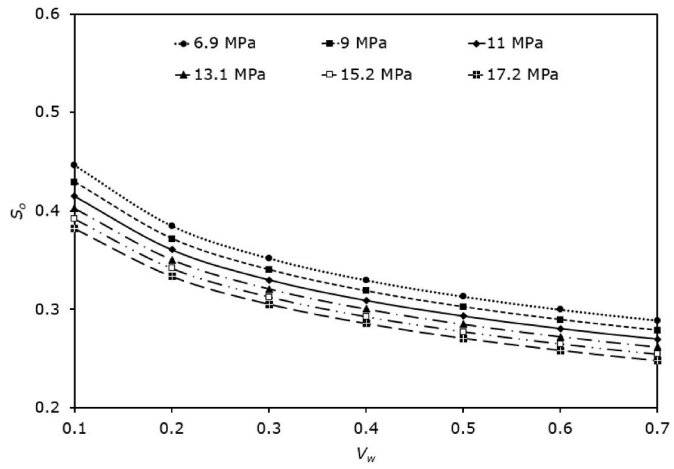

Fig. 13. Variations in oil saturation at the fracture-matrix interface for different water volume injection and stress loading.

4.3.3. Water and oil saturation

Injecting water in fractured reservoirs is one of the most common methods for enhanced oil recovery. When water is injected into fractured rocks, it pushes the oil out of the rock matrix. Thus, oil is being replaced by water in the rock. In order to better understand the dynamics of this phenomenon, especially when the rock is subjected to external load, water saturation (S_w) variations at the fracture-matrix interface, for different injected water volumes (V_w) values are shown in Fig. 12. It is evident from the figure that as water is injected into the fractured zone, its saturation increases. The same trend has been observed at different stress loading values considered in the present study. However, this increase in water saturation, as both injected water volume and external stress loading increases, is non-linear. Initially, between inkected water volume of 0.1 and 0.4, water saturation rises sharply, followed by a rather gradual increase. It is reasonable to expect that water saturation would increase as the injected water volume increases, as more water would be pumped into the fracture-matrix area. However, there is a limit to how much water can be held up in the pore volumes. Thus, after the initial sudden increase in water saturation, a further increase is more gradual. However, the increase in water saturation due to stress loading indicates the importance of external loading on the rock matrix for enhanced oil recovery.

As water is injected into the rock matrix, oil is pushed out, as shown in Fig. 13. For all stress loading values, it can be seen that oil saturation (S_o) reduces non-linearly as injected water volume increases. For stress loading of 6.9 MPa, as 10 % of water (by volume) is injected into the rock, the oil saturation is 44 %, however, increasing the injected water volume to 70 %, the oil saturation drops to 29 %. At the same time, for an external stress of 17.2 MPa and injected water volume of 70 %, the oil saturation is 24 %. Thus, by increasing the stress loading from 6.9 MPa to 17.2 MPa, an additional 5 % of oil is recovered from the fractured rock.

The spatial variations in oil saturation for various injected water values, during stress loading of 6.9 MPa and 17.2 MPa respectively, are shown in Figs. 14 and 15. Oil saturation fluctuations are displayed over the whole flow domain rather than only at the fracture-matrix interface. In the figure, water is injected from the left. As water is injected into the confined reservoir model, oil is seen to be displaced by it and retrieved at

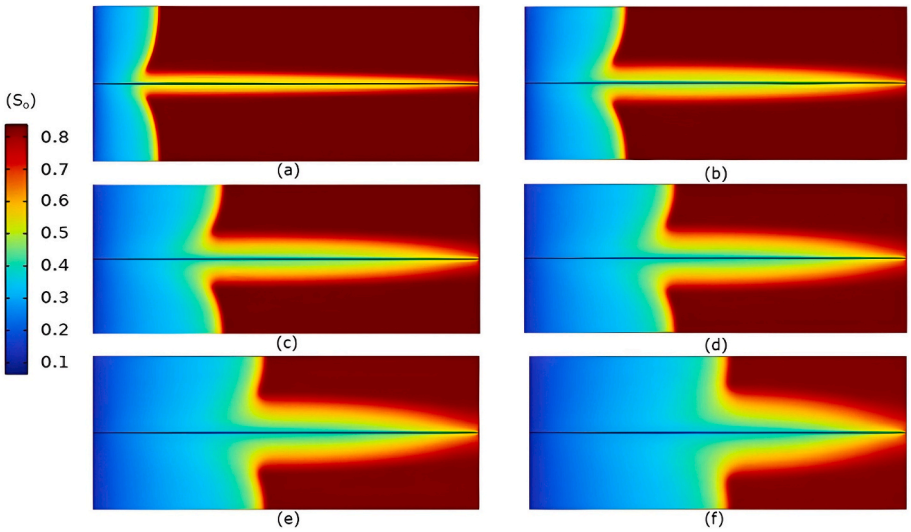

Fig. 14. Variations in oil saturation at stress loading of 6.9 MPa and for injected water volume of (a) 10 % (b) 20 % (c) 30 % (d) 40 % (e) 50 % (f) 70 %.

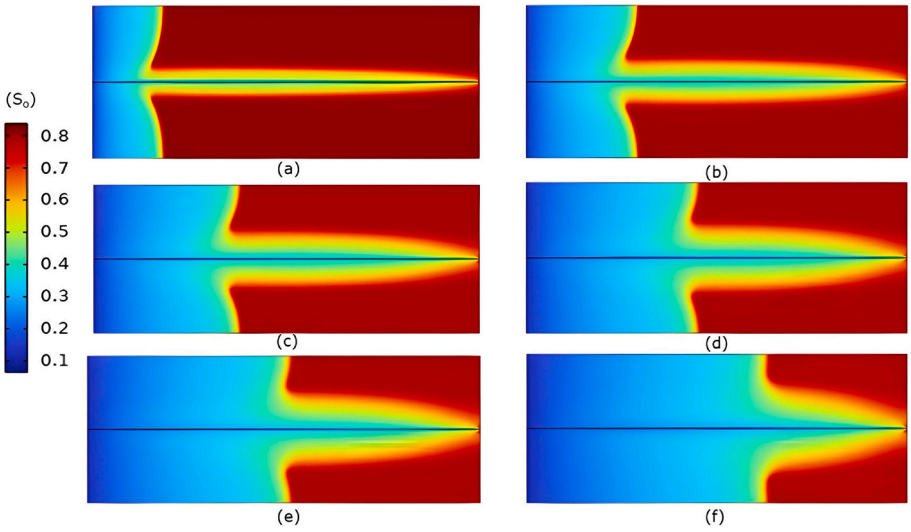

Fig. 15. Variations in oil saturation at stress loading of 17.2 MPa and for injected water volume of (a) 10 % (b) 20 % (c) 30 % (d) 40 % (e) 50 % (f) 70 %.

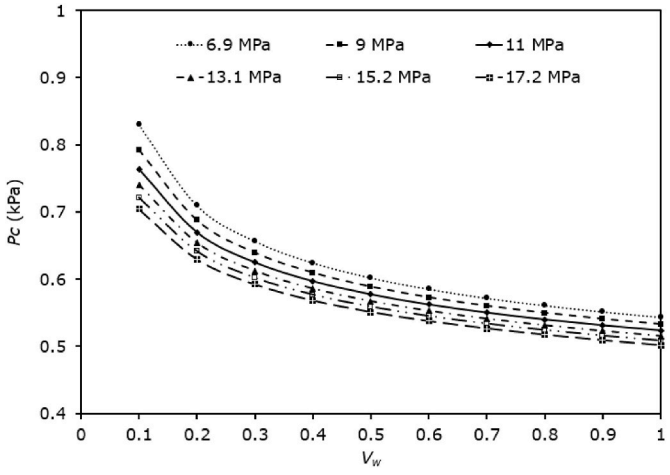

Fig. 16. Capillary pressure variations w.r.t water volume injection.

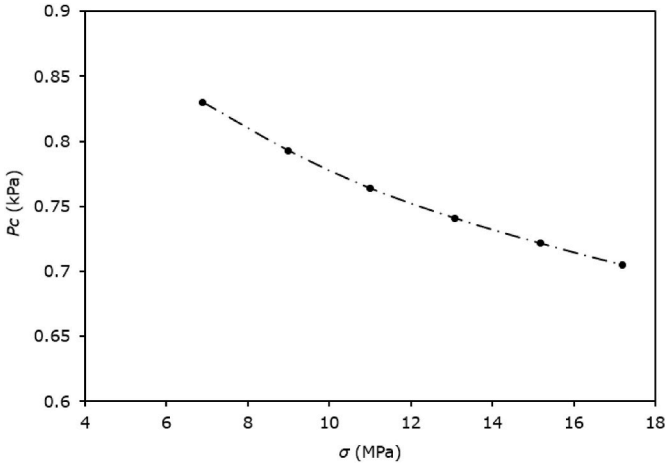

Fig. 17. Capillary pressure variations w.r.t. stress loading at $V_w = 0.1$.

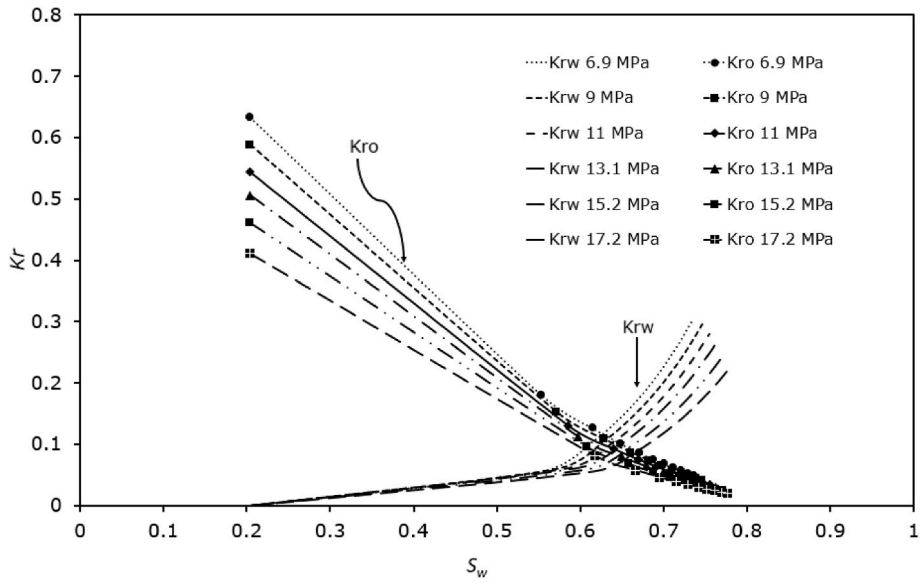

Fig. 18. Relative permeability w.r.t water saturation.

the flow domain's exit (right boundary). In terms of how stress loading affects oil recovery, it is evident that as stress loading increases, so does the amount of oil recovered at the exit. This is because when the stress loading increases, the fracture aperture decreases, and the overall volume of the fracture region decreases, which causes oil to be pushed out of the reservoir.

4.3.4. Capillary pressure

One of the most important flow parameters in the context of reservoir engineering is the capillary pressure (*Pc*). Variations of the capillary pressure with respect to the injected water volume are shown in Fig. 16. Capillary pressure has been plotted against the volume of injected water because it is a function of water saturation (*Sw*). The figure shows a nonlinear reduction in capillary pressure as the volume of injected water increases. This is because as water continues to flow into the fractured rocks, water saturation rises, causing a drop in the capillary pressure. Furthermore, it can be seen in Fig. 17 that as the stress loading increases, the capillary pressure decreases. This is because the fracture aperture decreases with an increase in external loading, resulting in lower capillary pressure. The published experimental data shows a similar pattern, showing an increase in water saturation with externally applied stress [57]. Therefore, it is evident that as the stress loading increases, the capillary pressure decreases almost linearly. These observations suggest that stress loading is crucial in controlling the fluid flow behaviour in fractured rock systems. The reduction in capillary pressure with stress loading also highlights the potential for enhancing fluid flow through fractured rocks by applying stress.

4.3.5. Relative permeability

Apart from the capillary pressure, the other crucial flow parameter in reservoir modelling is its relative permeability. The variations in relative permeabilities of water (Kr_w) and oil (Kr_o) at the fracture-matrix interface, under various stress-loading conditions, is shown in Fig. 18. It can be clearly seen in the figure that as the water saturation increases, the relative permeability of the oil decreases nonlinearly. Similarly, as water saturation increases, the oil relative permeability decreases. Relative permeability varies as applied stress varies. Water saturation also varies as the external loading varies. Thus, the relative permeability depends on both the stress loading and water saturation. It can be further observed that higher external stress loading results in higher water relative permeability and lower oil relative permeability. Lian et al. [57] observed a similar trend and reported that with an increase in external stress loading, the saturation of the wetting phase (water) increases, while the water relative permeability curves shift to the right. This indicates that the rock becomes increasingly water-wet as external stress increases.

5. Conclusions

A fully coupled numerical model for accurate estimation of enhanced oil recovery from fractured hydrocarbon reservoirs has been developed in this study by coupling Finite Element Method (FEM) and Computational Fluid Dynamics (CFD). Effects of externally applied stress loading on geomechanical and multiphase flow parameters of the rock matrix have been analysed using the well-validated fully-coupled numerical model. The results indicate that as applied stress loading on the rock matrix increases, its porosity and permeability decrease. Similarly, under the application of external loading, the fracture aperture decreases, which is consistent with real-world observations. The contribution of the intact rock to the determined strain and conductivity of the fractured core is found to be low due to minimal pore strain and low permeability. The capillary at the fracture-matrix interface has been observed to decrease due to increase in stress loading. This indicates that as stress loading increases, the fracture-matrix interface become water-wet, and the relative permeability curves shift toward the right. These results provide valuable insights into multiphase flow behaviour in naturally fractured rocks under externally applied stress and emphasize the importance of understanding these phenomena in various geological and engineering applications.

CRediT authorship contribution statement

Haval Kukha Hawez: Writing – original draft, Validation, Software, Methodology, Investigation, Formal analysis, Data curation, Conceptualization. **Taimoor Asim:** Writing – original draft, Supervision, Resources, Project administration, Methodology. **Marco Fazio:** Writing – original draft, Supervision, Methodology, Conceptualization.

Declaration of competing interest

The authors declare that they have no known competing financial interests or personal relationships that could have appeared to influence the work reported in this paper.

References

[1] S.P. Rodionov, A.A. Pyatkov, V.P. Kosyakov, Influence of fractures orientation on two-phase flow and oil recovery during stationary and non-stationary waterflooding of oil reservoirs, AIP Conf. Proc. 2027 (2018), https://doi.org/10.1063/1.5065138.

[2] A.H. Haghi, R. Chalaturnyk, Experimental characterization of hydrodynamic properties of a deformable rock fracture, Energies 15 (2022), https://doi.org/10.3390/en15186769.

[3] H.S. Viswanathan, J. Ajo-Franklin, J.T. Birkholzer, J.W. Carey, Y. Guglielmi, J. D. Hyman, et al., From fluid flow to coupled processes in fractured rock: recent advances and new frontiers, Rev. Geophys. 60 (2022) 1–65, https://doi.org/10.1029/2021RG000744.

[4] A.M. Kassa, S.E. Gasda, D. Landa-Marbán, T.H. Sandve, K. Kumar, Field-scale impacts of long-term wettability alteration in geological CO2 storage, Int. J. Greenh. Gas Control 114 (2022), https://doi.org/10.1016/j.ijggc.2021.103556.

[5] D.W. Carlson, K. Toda-Peters, A.Q. Shen, S.J. Haward, Volumetric evolution of elastic turbulence in porous media, J. Fluid Mech. 950 (2022) 1–21, https://doi.org/10.1017/jfm.2022.836.

[6] X. Rao, L. Cheng, R. Cao, P. Jia, P. Dong, X. Du, A modified embedded discrete fracture model to improve the simulation accuracy during early-time production of multi-stage fractured horizontal well. Soc. Pet. Eng. - SPE/IATMI Asia Pacific Oil Gas Conf. Exhib. 2019, APOG 2019, 2019, https://doi.org/10.2118/196263-ms. Bali, Indonesia.

[7] X. Liu, G. Zhu, T. Asim, Y. Zhang, R. Mishra, The innovative design of air caps for improving the thermal efficiency of CFB boilers, Energy 221 (2021) 119844, https://doi.org/10.1016/j.energy.2021.119844.

[8] P. Chen, M. Fiallos-Torres, Y. Xing, W. Yu, C. Guo, J. Leines-Artieda, et al., Water intrusion characterization in naturally fractured gas reservoir based on spatial DFN connectivity analysis, Energies 13 (2020), https://doi.org/10.3390/en13164235.

[9] B. Freegah, T. Asim, D. Albarzenji, S. Pradhan, R. Mishra, Effect of the shape of connecting pipes on the performance output of a closed-loop hot water solar Thermo-syphon, 3rd Int Work Congr EMaintenance (2014) 45–59.

[10] J. Jiang, J. Yang, Coupled fluid flow and geomechanics modeling of stress-sensitive production behavior in fractured shale gas reservoirs, Int. J. Rock Mech. Min. Sci. 101 (2018) 1–12, https://doi.org/10.1016/j.ijrmms.2017.11.003.

[11] H. Hawez, R. Sanaee, N.H. Faisal, Multiphase flow modelling in fractured reservoirs using a novel computational fluid dynamics approach. Pap. Present. 55th U.S. Rock Mech. Symp., Virtual, 2021 https://doi.org/ARMA-2021-1077.

[12] G. Cui, L. Zhu, Q. Zhou, S. Ren, J. Wang, Geochemical reactions and their effect on CO2 storage efficiency during the whole process of CO2 EOR and subsequent storage, Int. J. Greenh. Gas Control 108 (2021) 103335, https://doi.org/10.1016/j.ijggc.2021.103335.

[13] X. Li, K. Xiao, R. Wang, X. Li, Experimental research on enhanced oil recovery methods for gas injection of fractured reservoirs based on microfluidic chips, ACS Omega 7 (2022) 27382–27389, https://doi.org/10.1021/acsomega.2c02390.

[14] K. Weishaupt, V. Joekar-Niasar, R. Helmig, An efficient coupling of free flow and porous media flow using the pore-network modeling approach, J. Comput. Phys. X 1 (2019), https://doi.org/10.1016/j.jcpx.2019.100011.

[15] E. Rohan, J. Turjanicová, V. Lukeš, The Biot–Darcy–Brinkman model of flow in deformable double porous media; homogenization and numerical modelling, Comput. Math. Appl. 78 (2019) 3044–3066, https://doi.org/10.1016/j.camwa.2019.04.004.

[16] K. Baber, K. Mosthaf, B. Flemisch, R. Helmig, S. Müthing, B. Wohlmuth, Numerical Scheme for Coupling Two-phase Compositional Porous-Media Flow and One-phase Compositional Free Flow, 77, IMA J Appl Math (Institute Math Its Appl, 2012, pp. 887–909, https://doi.org/10.1093/imamat/hxs048.

[17] A. Borio, A. Fumagalli, S. Scialò, Comparison of the response to geometrical complexity of methods for unstationary simulations in discrete fracture networks with conforming, polygonal, and non-matching grids, Comput. Geosci. 25 (2021) 143–162, https://doi.org/10.1007/s10596-020-09996-9.

[18] F.J. Carrillo, I.C. Bourg, C. Soulaine, Multiphase flow modeling in multiscale porous media: an open-source micro-continuum approach, J. Comput. Phys. X 8 (2020) 100073, https://doi.org/10.1016/j.jcpx.2020.100073.

[19] D. Sijacic, P. Fokker, Simulation of flow , thermal and mechanical effects in COMSOL for enhanced geothermal systems, COMSOL Conf (2013 Rotterdam 2013) 1–4.

[20] M.N. Tarhuni, W.R. Sulaiman, M.Z. Jaafar, M. Milad, A.M. Alghol, A review of the dynamic modeling approaches for characterizing fluid flow in naturally fractured reservoirs, Energy Eng. J. Assoc. Energy Eng. 118 (2021) 761–795, https://doi.org/10.32604/EE.2021.016645.

[21] H.K. Hawez, R. Sanaee, N.H. Faisal, A critical review on coupled geomechanics and fluid flow in naturally fractured reservoirs, J. Nat. Gas Sci. Eng. 95 (2021) 104150, https://doi.org/10.1016/j.jngse.2021.104150.

[22] J.E. Warren, P.J. Root, The behavior of naturally fractured reservoirs, Soc. Petrol. Eng. J. 3 (1963) 245–255, https://doi.org/10.2118/426-pa.

[23] D. Singh, M. Charlton, T. Asim, R. Mishra, A. Townsend, L. Blunt, Quantification of additive manufacturing induced variations in the global and local performance characteristics of a complex multi-stage control valve trim, J. Pet. Sci. Eng. 190 (2020), https://doi.org/10.1016/j.petrol.2020.107053.

[24] A. Moinfar, W. Narr, M.H. Hui, B. Mallison, S.H. Lee, Comparison of discrete-fracture and dual-permeability models for multiphase flow in naturally fractured reservoirs, in: SPE Reserv. Simul. Symp., 63, Society of Petroleum Engineers, Woodlands, Texas, USA, 2011, pp. 84–85, https://doi.org/SPE-142295-MS.

[25] H. Kazemi, L.S. Merrill, K.L. Porterfield, P.R. Zeman, Numerical simulation of water-oil flow in naturally fractured reservoirs, Soc Pet Eng AIME J 16 (1976) 317–326, https://doi.org/10.2118/5719-pa.

[26] R.H. Rossen, Simulation of naturally fractured reservoirs with semi-implicit source terms, SPE J. 17 (1977) 201–210, https://doi.org/10.2118/5737-PA.

[27] A.M. Saidi, Simulation of naturally fractured reservoirs, Pap. Present. SPE Reserv. Simul. Symp. (1983), https://doi.org/10.2118/15627-PA. San Francisco, California.

[28] J.R. Gilman, An efficient finite-difference method for simulating phase segregation in the matrix blocks in double-porosity reservoirs, SPE Reserv Eng (Society Pet Eng 1 (1986) 403–413, https://doi.org/10.2118/12271-PA.

[29] K. Pruess, T.N. Narasimhan, Practical method for modeling fluid and heat flow in fractured porous media, Soc. Petrol. Eng. J. 25 (1985) 14–26, https://doi.org/10.2118/10509-pa.

[30] A.C. Hill, G.W. Thomas, New approach for simulating complex fractured reservoirs, Soc Pet Eng AIME, SPE (1985) 429–440, https://doi.org/10.2523/13537-ms.

[31] X. Liu, T. Asim, G. Zhu, R. Mishra, Theoretical and experimental investigations on the combustion characteristics of three components mixed municipal solid waste, Fuel 267 (2020) 117183, https://doi.org/10.1016/j.fuel.2020.117183.

[32] E. Ukar, S.E. Laubach, J.N. Hooker, Outcrops as guides to subsurface natural fractures: example from the Nikanassin Formation tight-gas sandstone, Grande Cache, Alberta foothills, Canada, Mar. Petrol. Geol. 103 (2019) 255–275, https://doi.org/10.1016/j.marpetgeo.2019.01.039.

[33] Z.D. Yang, Y. Wang, X.Y. Zhang, M. Qin, S.W. Su, Z.H. Yao, et al., Numerical simulation of a horizontal well with multi-stage oval hydraulic fractures in tight oil reservoir based on an embedded discrete fracture model, Front. Energy Res. 8 (2020) 1–12, https://doi.org/10.3389/fenrg.2020.601107.

[34] T. Asim, R. Mishra, K. Ubbi, K. Zala, Computational fluid dynamics based optimal design of vertical axis marine current turbines, Procedia CIRP 11 (2013) 323–327, https://doi.org/10.1016/j.procir.2013.07.023.

[35] P. Cheng, W. Shen, Q. Xu, X. Lu, C. Qian, Y. Cui, Multiphysics coupling study of near-wellbore and reservoir models in ultra-deep natural gas reservoirs, J. Pet. Explor. Prod. Technol. (2022), https://doi.org/10.1007/s13202-021-01424-7.

[36] H.K. Hawez, T. Asim, Impact of regional pressure dissipation on carbon capture and storage projects: a comprehensive review, Energies 17 (2024) 1889, https://doi.org/10.3390/en17081889.

[37] W. Shen, T. Ma, X. Li, B. Sun, Y. Hu, J. Xu, Fully coupled modeling of two-phase fluid flow and geomechanics in ultra-deep natural gas reservoirs, Phys. Fluids 34 (2022), https://doi.org/10.1063/5.0084975.

[38] M. Shen, F. Kong, L. Tong, Y. Luo, S. Yin, C. Liu, et al., Carbon capture and storage (CCS): development path based on carbon neutrality and economic policy, Carbon Neutrality 1 (2022) 1–21, https://doi.org/10.1007/s43979-022-00039-z.

[39] G. Cui, W. Cheng, W. Xiong, T. Chen, Y. Li, X.T. Feng, et al., Influence of well types on optimizing the Co-production of gas from coal and tight formations, Energy Fuel. 36 (2022) 6736–6754, https://doi.org/10.1021/acs.energyfuels.2c00124.

[40] H.R. Kukha Hawez, Coupled Geomechanics and Transient Multiphase Flow at Fracture-Matrix Interface in Tight Reservoirs, Robert Gordon University, PhD thesis, 2023, https://doi.org/10.48526/rgu-wt-1987869. Hosted on OpnAIR [online].

[41] COMSOL, Subsurface Flow Module User Guide, 2022, Version 6.0.

[42] R.H. Brooks, A.T. Corey, Properties of porous media affecting fluid flow, J. Irrigat. Drain. Div. 92 (1966) 61–88.

[43] J.A. Franklin, Suggest methods for determining water content, porosity, density, absorption and related properties and swelling and slake-durability index properties, Int. J. Rock Mech. Min. Sci. Geomech. Abstr. (1979) 141–156.

[44] X. Ren, Y. Zhao, Q. Deng, J. Kang, D. Li, D. Wang, A relation of hydraulic conductivity — void ratio for soils based on Kozeny-Carman equation, Eng. Geol. 213 (2016) 89–97, https://doi.org/10.1016/j.enggeo.2016.08.017.

[45] R. Sanaee, G.F. Oluyemi, M. Hossain, M.B. Oyeneyin, Stress effects on flow partitioning in fractured reservoirs: equivalent porous media versus poro-elasticity coupled modeling, in: 447th U.S. Rock Mech. Symp. 23-26 June 2013, 3, American Rock Mechanics Association, San Francisco, California, 2013, pp. 2329–2337, https://doi.org/ARMA-2013-442.

[46] M. Bai, D. Elsworth, Modeling of subsidence and stress-dependent hydraulic conductivity for intact and fractured porous media, Rock Mech. Rock Eng. 27 (1994) 209–234, https://doi.org/10.1007/BF01020200.

[47] I.I. Bogdanov, V.V. Mourzenko, J.F. Thovert, P.M. Adler, Effective permeability of fractured porous media in steady state flow, Water Resour. Res. 39 (2003) 1–16, https://doi.org/10.1029/2001WR000756.

[48] J. Zhang, W.B. Standifird, J.C. Roegiers, Y. Zhang, Stress-dependent fluid flow and permeability in fractured media: from lab experiments to engineering applications, Rock Mech. Rock Eng. 40 (2007) 3–21, https://doi.org/10.1007/s00603-006-0103-x.

[49] P. Knabner, L. Angermann, Numerical Methods for Elliptic and Parabolic Partial Differential Equations, 44, Springer International Publishing, Cham, 2021, https://doi.org/10.1007/978-3-030-79385-2.

[50] C.F. Babbs, The origin of Korotkoff sounds and the accuracy of auscultatory blood pressure measurements, J Am Soc Hypertens 9 (2015) 935–950.e3, https://doi.org/10.1016/j.jash.2015.09.011.

[51] E. Longatte, F. Baj, Y. Hoarau, M. Braza, D. Ruiz, C. Canteneur, Advanced numerical methods for uncertainty reduction when predicting heat exchanger dynamic stability limits: review and perspectives, Nucl. Eng. Des. 258 (2013) 164–175, https://doi.org/10.1016/j.nucengdes.2012.12.003.

[52] R. Stalker, G.M. Graham, G. Oluyemi, Modelling staged diversion treatments and chemical placement in the presence of near-wellbore fractures, Proc. - SPE Int. Sysposium Oilfield Chem. 2 (2009) 745–757, https://doi.org/10.2118/121683-ms.

[53] K. Su, J.P. Latham, D. Pavlidis, J. Xiang, F. Fang, P. Mostaghimi, et al., Multiphase flow simulation through porous media with explicitly resolved fractures, Geofluids 15 (2015) 592–607, https://doi.org/10.1111/gfl.12129.
[54] A.H. Haghi, R. Chalaturnyk, S. Geiger, New semi-analytical insights into stress-dependent spontaneous imbibition and oil recovery in naturally fractured carbonate reservoirs, Water Resour. Res. 54 (2018) 9605–9622, https://doi.org/10.1029/2018WR024042.
[55] N. Cao, G. Lei, P. Dong, H. Li, Z. Wu, Y. Li, Stress-Dependent permeability of fractures in tight reservoirs, Energies 12 (2019), https://doi.org/10.3390/en12010117.
[56] P. Bagherzadeh, K. Goshtasbi, E. Kazemzadeh, M. Kashef, H. Aloki Bakhtiari, Stress-dependence of the permeability, porosity, and compressibility in fractured porous media regarding fracturing condition, Bull. Eng. Geol. Environ. 80 (2021) 5091–5110, https://doi.org/10.1007/s10064-021-02215-4.
[57] P.Q. Lian, L.S. Cheng, C.Y. Ma, The characteristics of relative permeability curves in naturally fractured carbonate reservoirs, J. Can. Pet. Technol. 51 (2012) 137–142, https://doi.org/10.2118/154814-PA.